Supplementary Materials

Precise and scalable fabrication of metal pair-site catalysts enabled by intramolecular integrated donor atoms

Yuqing Chen,[1] Shanshan Qiao,[2] Yanhong Tang, [2,*] Yi Du,[1] Danyu Zhang,[1] Wenjie Wang,[1] Haijiao Xie[3] and Chengbin Liu[1,**]

[1]Hunan University, State Key Laboratory of Chemo/Biosensing and Chemometrics, People's Republic of China

[2]Hunan University, College of Materials Science and Engineering, People's Republic of China

[3]Hangzhou Yanqu Information Technology Co., Ltd, People's Republic of China

*Correspondence: chem_cbliu@hnu.edu.cn

**Correspondence: tangyh@hnu.edu.cn

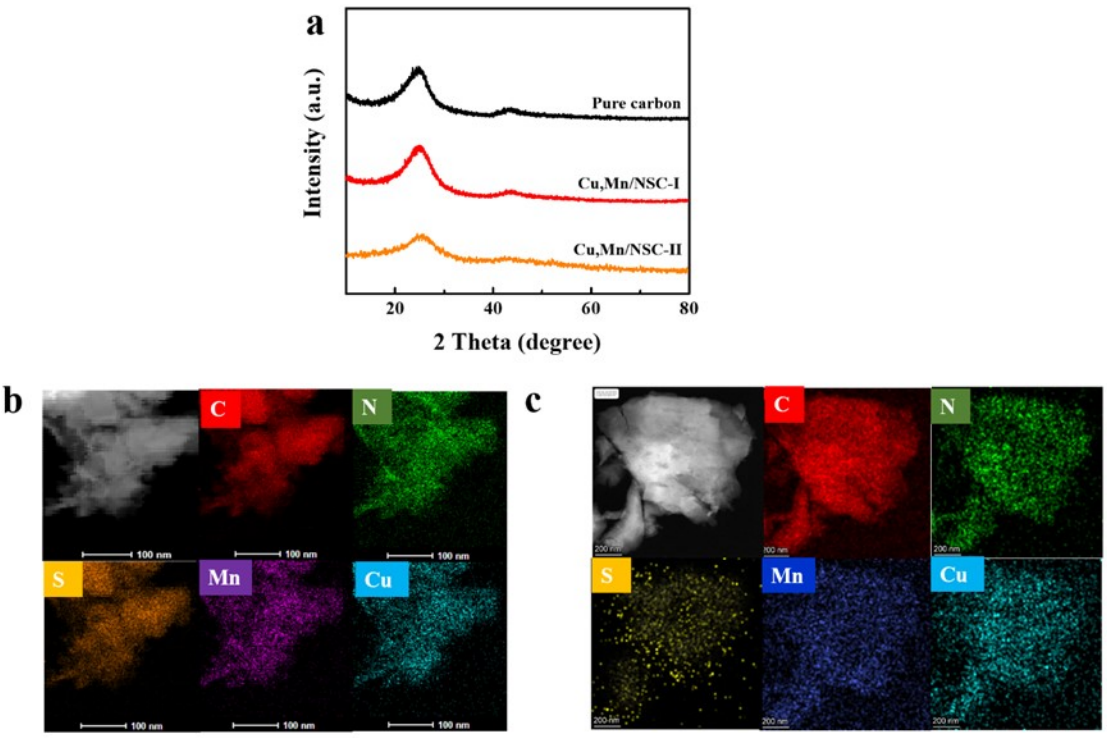

Figure S1. XRD patterns of pure carbon, Cu,Mn/NSC-I and Cu,Mn/NSC-II (a). TEM and STEM images with element mapping of Cu,Mn/NSC-I (a) and Cu,Mn/NSC-II (b). The resultant product was marked as Cu,Mn/NSC-I and Cu,Mn/NSC-II, respectively. As shown in **Figure S1a**, Cu,Mn/NSC-I and Cu,Mn/NSC-II only show two broad peaks at approximate 2θ values of 24 and 43° which are identified as (002) and (101) planes of amorphous carbons, suggesting the non-formation of metallic and oxide crystals on NSC-I and NSC-II. In **Figure S1b** and **c**, the amorphous carbon can be observed in both TEM images of Cu,Mn/NSC-I and Cu,Mn/NSC-II. The element mapping results of N, S, Cu and Mn reveal that these elements are homogeneously distributed in Cu,Mn/NSC-I and Cu,Mn/NSC-II. The results obtained from XRD, TEM and STEM coupled with element mapping analysis indicate that the Cu and Mn species are highly dispersed in NSC-I and NSC-II architecture.

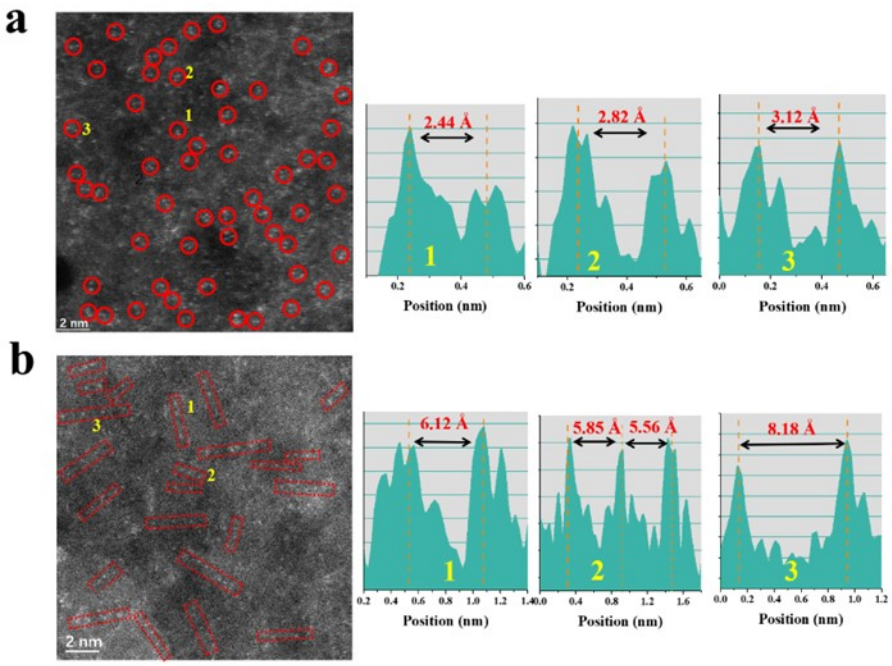

Figure S2. HAADF-STEM images of (Cu,Mn)/NSC-I (a) and (Cu,Mn)/NSC-II (b) with intensity profiles obtained in areas labeled 1, 2 and 3 and corresponding distance distribution of bright spots.

Table S1. The element content in NSC from elemental analyzer.

Samples	C (wt %)	N (wt %)	S (wt %)	O (wt %)	H (wt %)
NSC	89.03	2.54	1.74	5.61	1.08

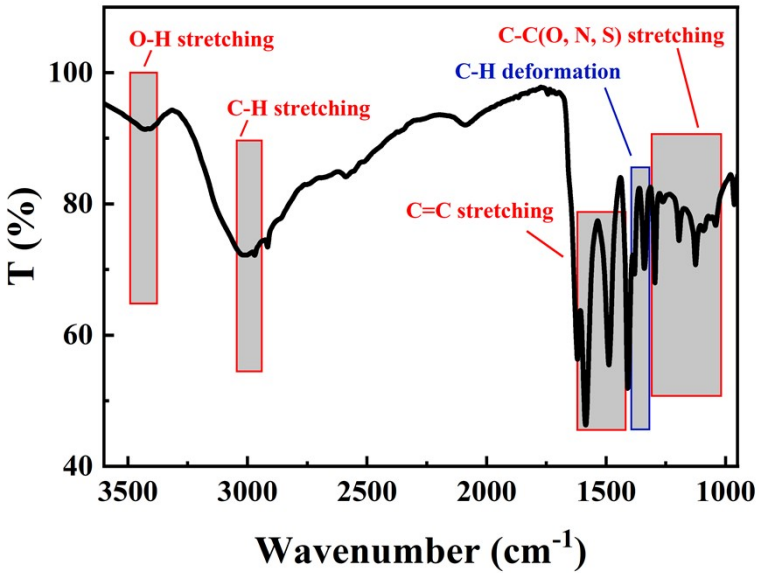

Figure S3. FTIR spectrum of NSC derived from houttuynia cordata.

Table S2. The experimental details of (Cu,Mn)/NSC preparation with different Cu/Mn molar ratio, different metal amounts and pyrolysis temperature (T_p).

Samples	Cu:Mn molar ratio	CuPc (mg)	MnPc (mg)	NSC (mg)	T_p(°C)
(Cu,Mn)/NSC(1:1)-800[a]	Cu : Mn = 1:1	70	70	100	800
(Cu,Mn)/NSC(1:2)-800	Cu : Mn = 1:2	70	140	100	800
(Cu,Mn)/NSC(2:1)-800	Cu : Mn = 2:1	140	70	100	800
(Cu,Mn)/NSC(1:1)-120	Cu : Mn = 1:1	120	120	100	800
(Cu,Mn)/NSC(1:1)-70 [a]	Cu : Mn = 1:1	70	70	100	800
(Cu,Mn)/NSC(1:1)-30	Cu : Mn = 1:1	30	30	100	800
(Cu,Mn)/NSC(1:1)-800 [a]	Cu : Mn = 1:1	70	70	100	800
(Cu,Mn)/NSC(1:1)-700	Cu : Mn = 1:1	70	70	100	700
(Cu,Mn)/NSC(1:1)-600	Cu : Mn = 1:1	70	70	100	600

a: The samples were prepared under the same conditions.

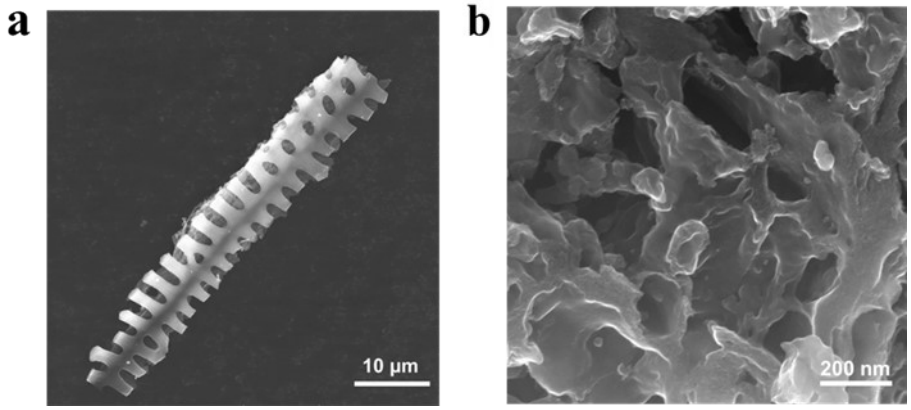

Figure S4. SEM (a) image of pristine NSC without ball milling and (b) (Cu,Mn)/NSC.

Table S3. Surface area and porosity of samples

Samples	**S_{BET} (m^2 g^{-1})**	**V_{total} (cm^3 g^{-1})**	**Pore Size (nm)**
NSC	33	0.052	16.15
(Cu,Mn)/ NSC	252	0.16	5.49

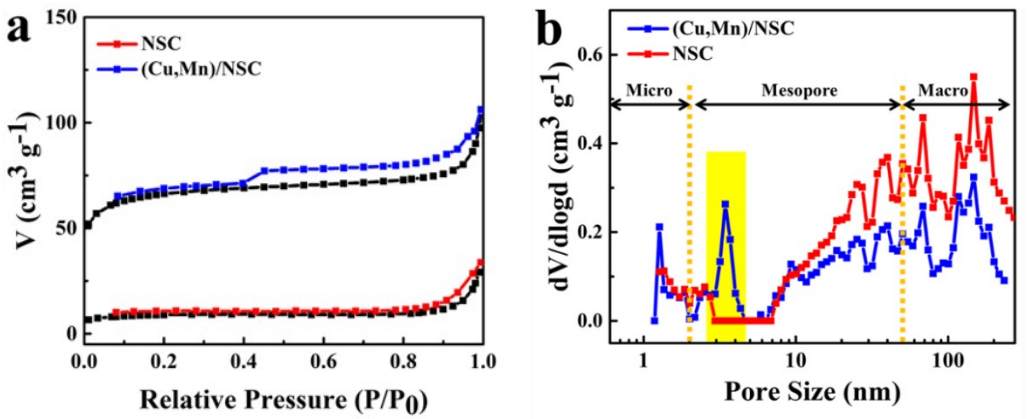

Figure S5. N_2 adsorption-desorption isotherms and pore size distribution of NSC and (Cu,Mn)/NSC.

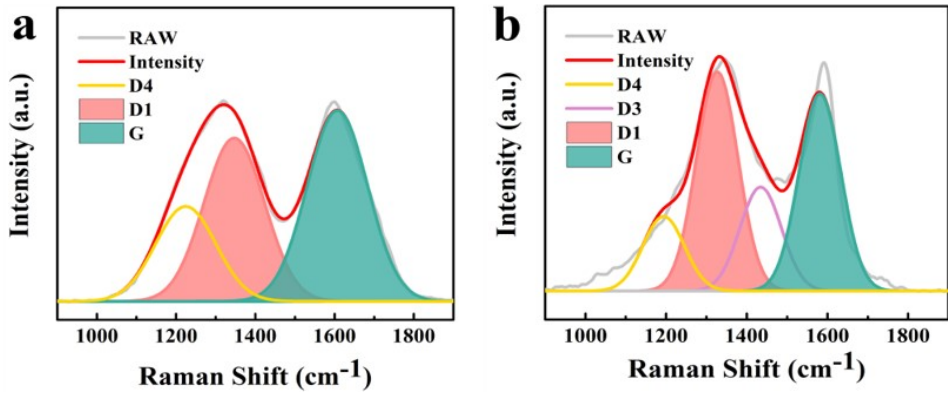

Figure S6. Raman spectra of NSC (a) and (Cu,Mn)/NSC (b).

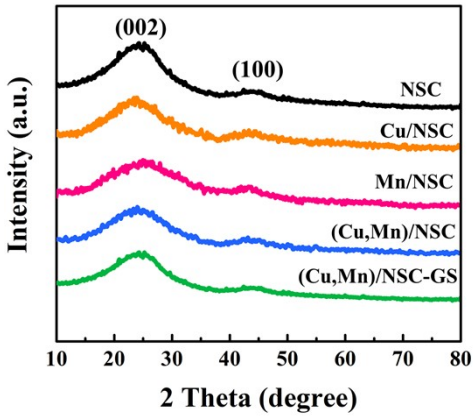

Figure S7. The XRD patterns of NSC, Cu/NSC, Mn/NSC and (Cu,Mn)/NSC. Two characteristic carbon (002) and (100) diffractions are ascribed to the NSC support. No diffraction peak related to crystalline metal species, such as nanoparticles, metal-based compounds, were observed.

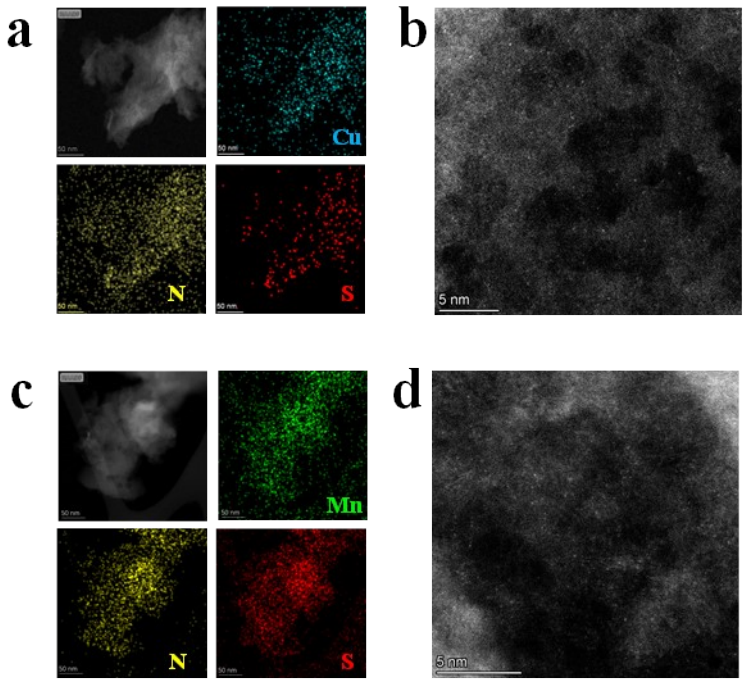

Figure S8. SACHAADF-STEM images with metal element mapping of Cu/NSC and Mn/NSC.

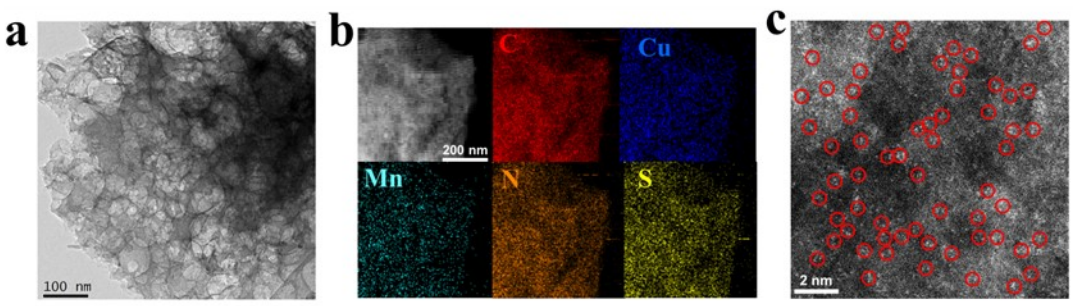

Figure S9. (Cu,Mn)/NSC-GS: (a) TEM image, (b) STEM image with element mapping, and (c) SACHAADF-STEM image with (d) magnified size. The atomic dispersion of Cu and Mn species were retained in (Cu,Mn)/NSC-GS.

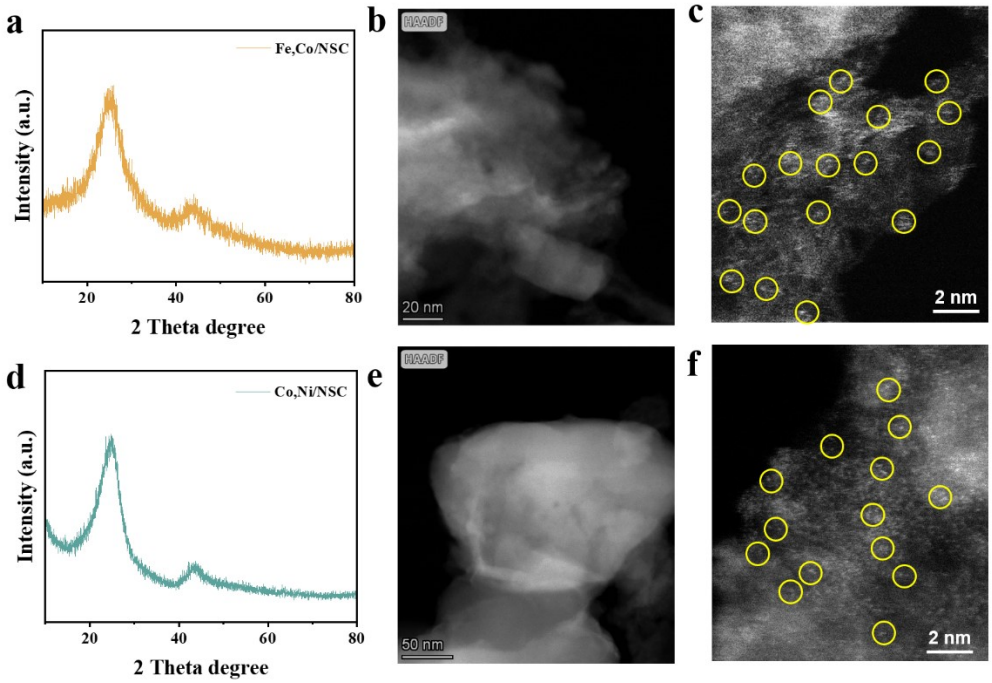

Figure S10. XRD patterns of Fe,Co/NSC (a) and Co,Ni/NSC (d) catalysts synthesized by the developed strategy. Corresponding HAADF-STEM images of Fe,Co/NSC (b) (c) and Co,Ni/NSC (e), (f). Fe,Co/NSC and Co,Ni/NSC were further fabricated by the developed strategy. The synthesis route was as same as that of (Cu,Mn)/NSC, but different metal precursors were used. XRD patterns (a and d) of Fe,Co/NSC and Co,Ni/NSC showed no obvious peaks due to metal-related nanoparticles, indicating high dispersion of metal-based species. To uncover the existing state of the metal species in Fe,Co/NSC and Co,Ni/NSC, we performed HAADF-STEM. As demonstrated in **Figure S10b**, no Fe,Co derived nanoparticles or nanoclusters can be found. The Fe,Co species were atomically dispersed on the N/S-co-doped nanocarbon architecture (**Figure S10c**). The existing state of the metal species in Co,Ni/NSC were also investigated, and the results were shown in **Figure S10e** and **f**. The Co,Ni species were confirmed atomically dispersed.

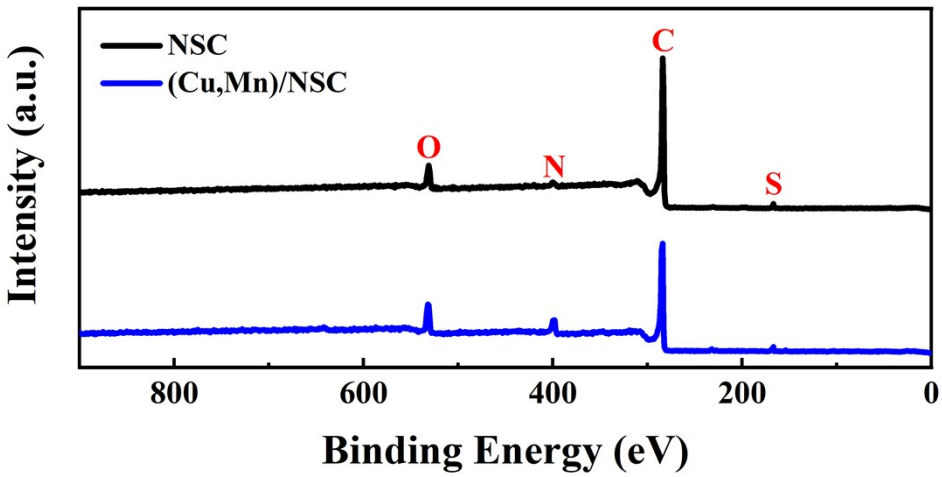

Figure S11. XPS spectra of survey scan for NSC and (Cu,Mn)/NSC.

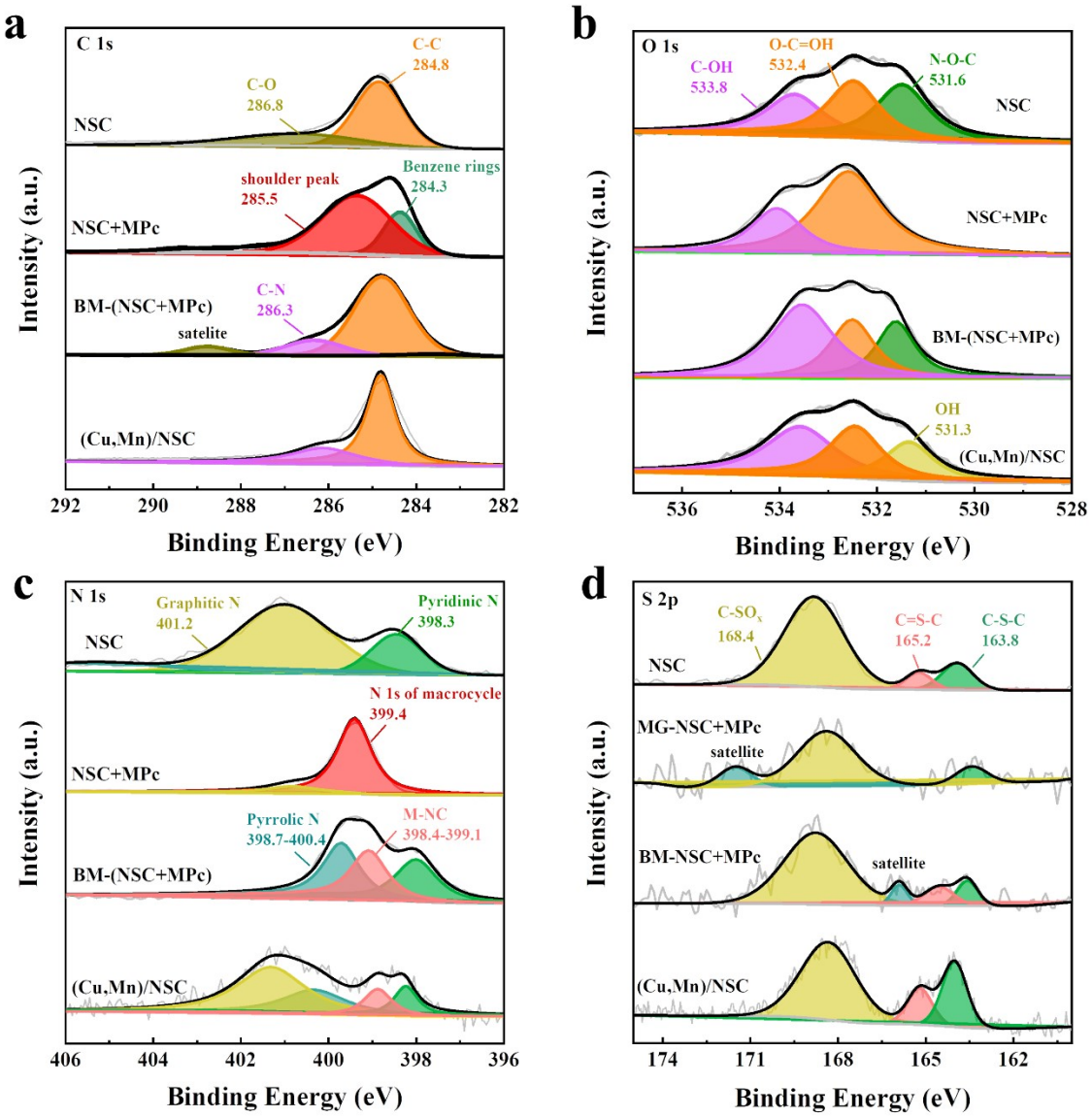

Figure S12. XPS spectra of (a) survey scan, (b) C 1s, (c) O 1s, (d)N 1s, and (e) S 2p for NSC, NSC+MPc, BM-(NSC+MPc) and (Cu,Mn)/NSC. NSC+MPc was prepared by grinding 100 mg NSC and 70 mg MPc (the molar ratio of MnPc : CuPc=1:1) manually for 2min. And the preparation of BM-(NSC+MPc) was as same as that of (Cu,Mn)/NSC but without pyrolysis.

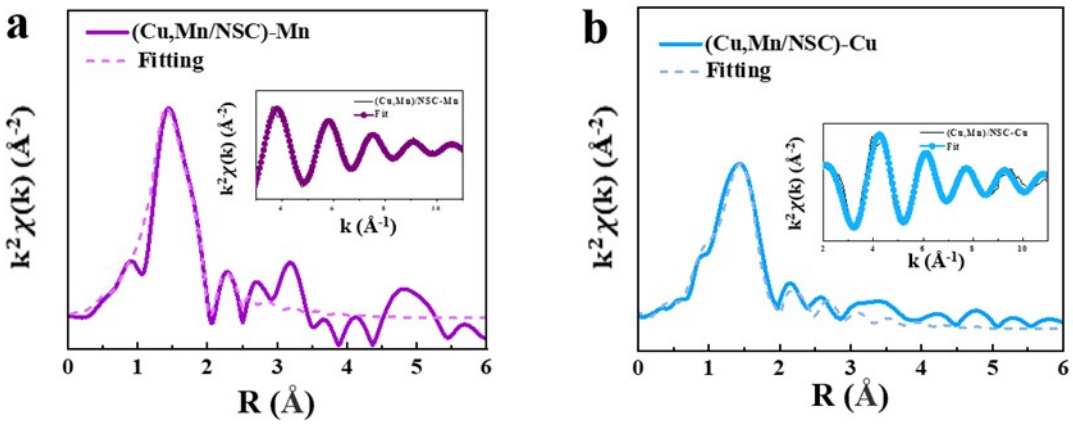

Figure S13. FT-EXAFS fitting curves at Mn K-edge (a) and Cu K-edge (b) with the corresponding structural model of (Cu,Mn)/NSC.

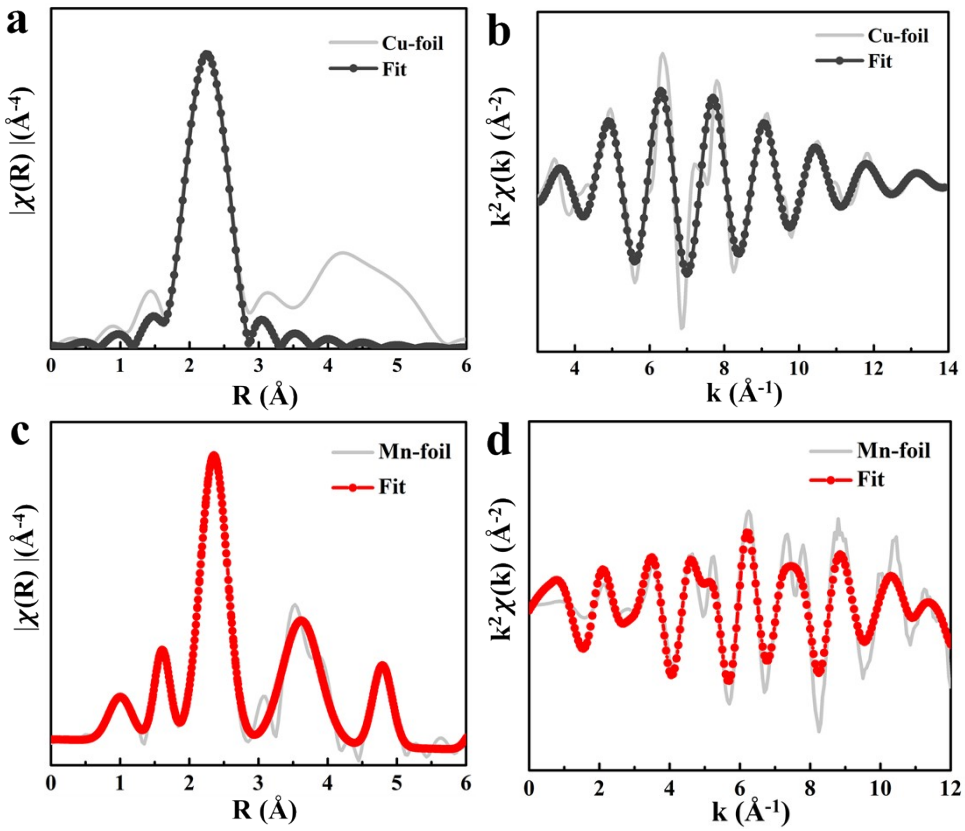

Figure S14. EXAFS fitting curves of (a and b) Cu foil and (c and d) Mn foil.

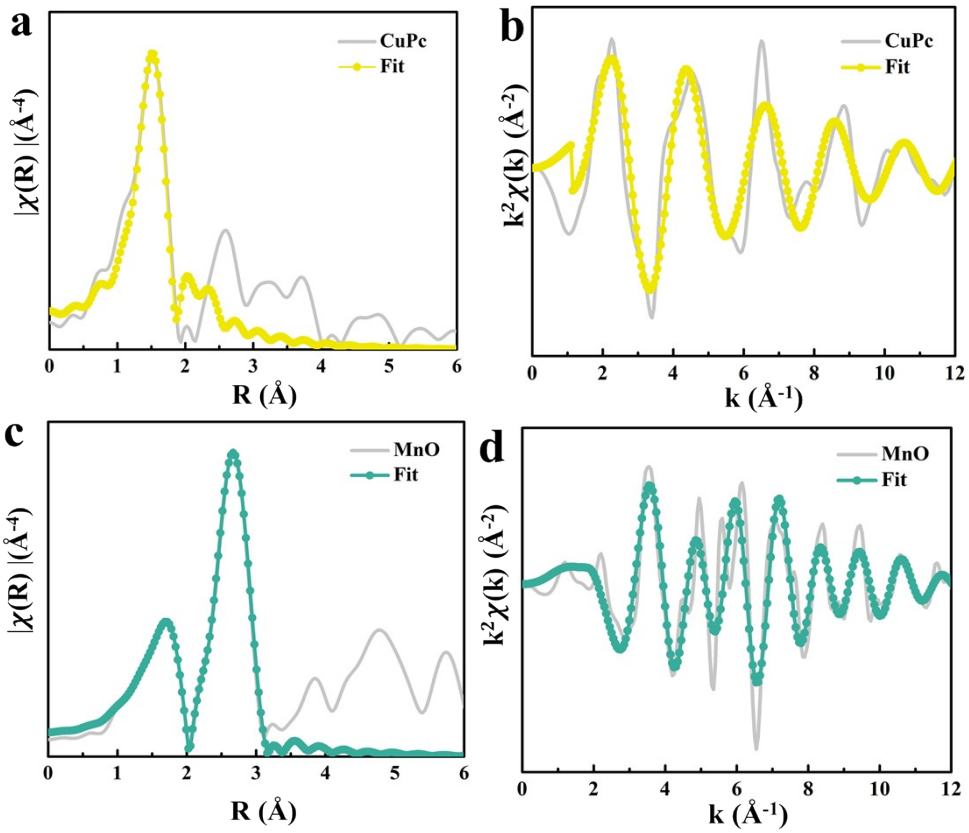

Figure S15. EXAFS fitting curves of (a and b) CuPc and (c and d) MnO.

Table S4. Structural parameters of (Cu,Mn)/NSC extracted from the EXAFS fitting (S_0^2=0.75).

Sample	Path	CN	R(Å)	$\sigma^2(10^{-3}Å^2)$	R factor
Cu foil	Cu-Cu	12	2.56±0.01	8.94	0.002
CuPc	Cu-N	4	1.94±0.01	2.96	0.01
Mn foil	Mn-Mn	12*	2.39±0.01	2.01	0.005
MnO	Mn-O	6	2.21±0.01	9.50	0.003
	Mn-Mn	12	3.12±0.007	8.64	
Cu-(Cu,Mn)/NSC	Cu-N	1.07±0.47	1.68±0.02	8.41	0.05
	Cu-S	2.01±0.77	2.27±0.02	8.41	
	Cu-C	0.65±0.41	2.15±0.02	9.03	
	Cu-Mn	0.87±0.35	2.45±0.02	9.52	
Mn-(Cu,Mn)/NSC	Mn-N	3.42±0.64	2.11±0.01	6.68	0.02
	Mn-S	0.57±0.16	2.18±0.008	6.68	
	Mn-Cu	0.65±0.12	2.42±0.01	9.43	

S_0^2 is the amplitude reduction factor; CN is the coordination number; R is interatomic distance (the bond length between metal central atoms and surrounding coordination atoms); σ^2 is Debye-Waller factor (a measure of thermal and static disorder in absorber-scatterer distances); ΔE_0 is edge-energy shift (the difference between the zero kinetic energy value of the sample and that of the theoretical model). R factor is used to value the goodness of the fitting.

* This value was fixed during EXAFS fitting, based on the known structure of Mn foil. Error bounds that characterize the structural parameters obtained by EXAFS spectroscopy were estimated as N ± 20%; R ± 1%; σ^2 ± 20%; ΔE_0 ± 20%.

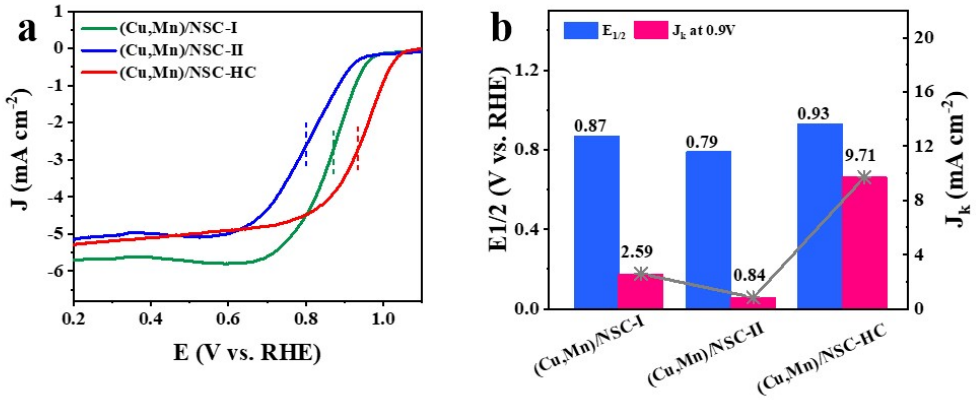

Figure S16. ORR polarization plots of samples involved different carbon support anchored metal species (a). Corresponding J_k at 0.9 V and $E_{1/2}$ (b). As can be seen, the ORR activity follows the trend of (Cu,Mn)/NSC-HC＞ (Cu,Mn)/NSC-I＞(Cu,Mn)/NSC-II.

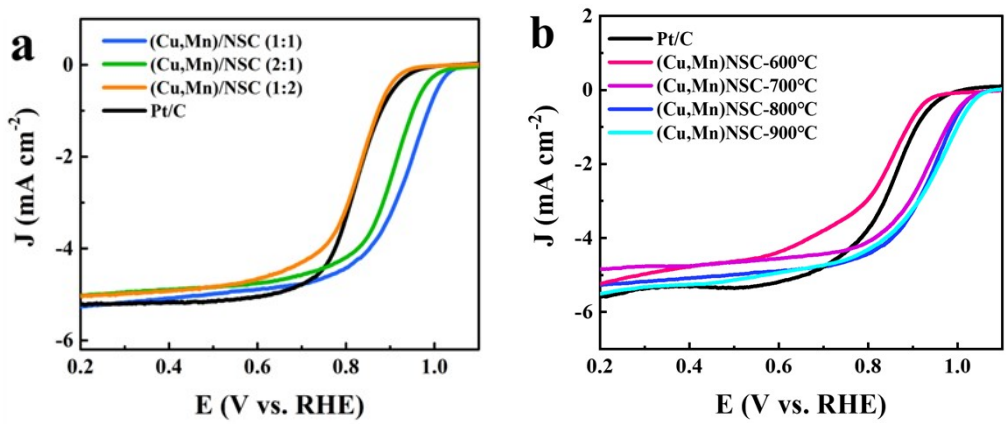

Figure S17. ORR polarization plots of (Cu,Mn)/NSC prepared (a) using different Cu:Mn molar ratios at 800°C and (b) at different pyrolysis temperatures keeping a Cu:Mn molar ratio of 1:1. Little promotion of ORR performance was observed over (Cu,Mn)/NSC-900°C. In the view of energy-saving, 800 °C was selected as the optimal temperature for (Cu,Mn)/NSC electrocatalysts.

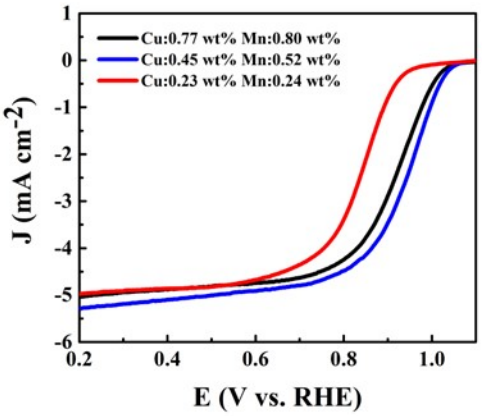

Figure S18. ORR polarization plots of (Cu,Mn)/NSC with different Cu/Mn content, in which the metal amount of different sample was determined by ICP-MS measurement. Cu: 0.77 wt% Mn: 0.80 wt% for (Cu,Mn)/NSC(1:1)-120; Cu: 0.45 wt% Mn: 0.52 wt% for (Cu,Mn)/NSC(1:1)-70; Cu: 0.23 wt% Mn: 0.24 wt% for (Cu,Mn)/NSC(1:1)-30.

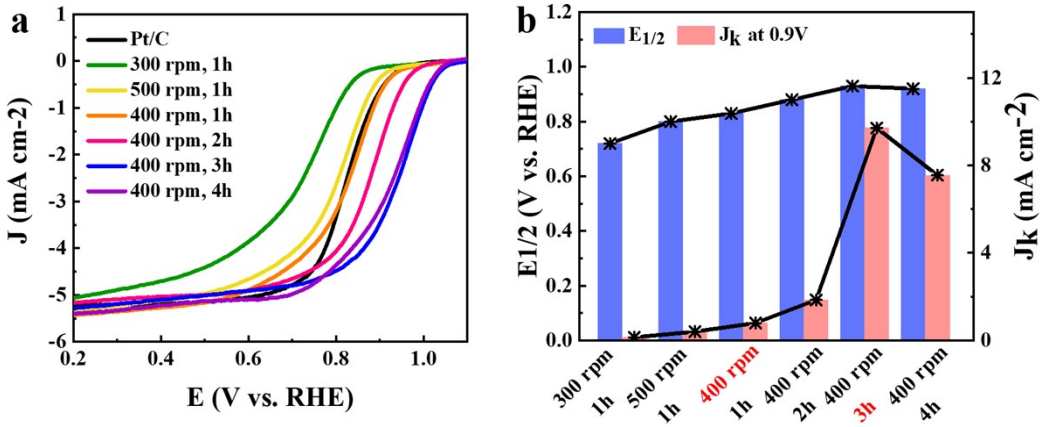

Figure S19. The optimal ball milling parameter for ORR activity.

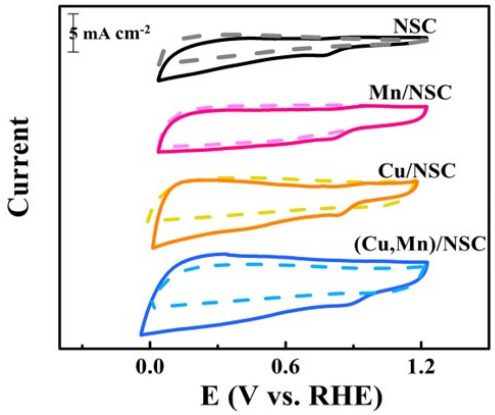

Figure S20. CV curves of (Cu,Mn)/NSC and other reference samples in O_2 (solid line) and N_2 (dash line)-saturated 0.1M KOH electrolyte at a scan rate of 50 mV/s.

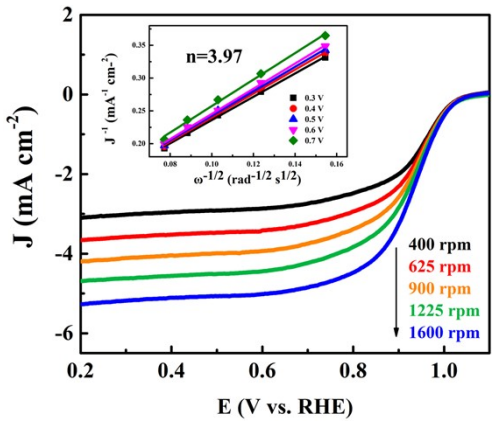

Figure S21. RDE polarization curves of (Cu,Mn)/NSC-GS at different rotating speeds. Inset is the K-L plots at different potentials.

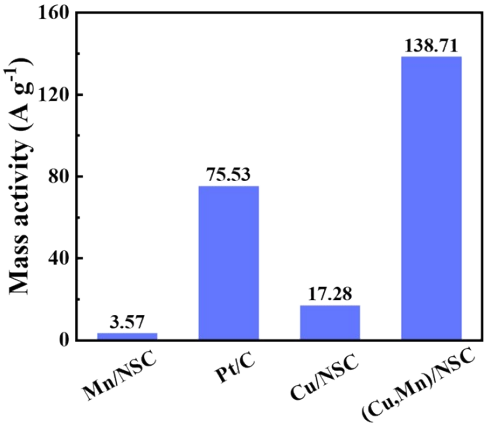

Figure S22. The mass activities obtained at J_k=0.9 V vs. RHE.

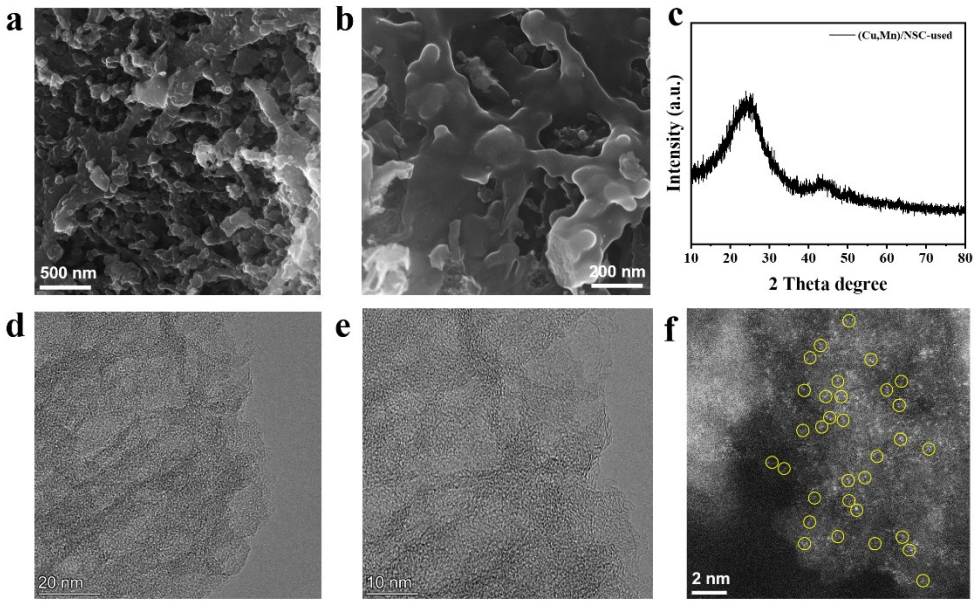

Figure S23 (a) and (b) SEM images of used (Cu,Mn)/NSC after cycling stability test. (c) Corresponding XRD patterns, (d,e) TEM images and (f) HADDF-STEM images.

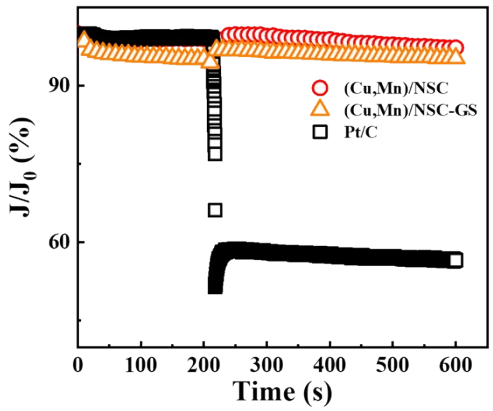

Figure S24. Plots of current density vs. time measured by chronoamperometry technique with the injection of 3 mL of methanol. Methanol was added around 200 s.

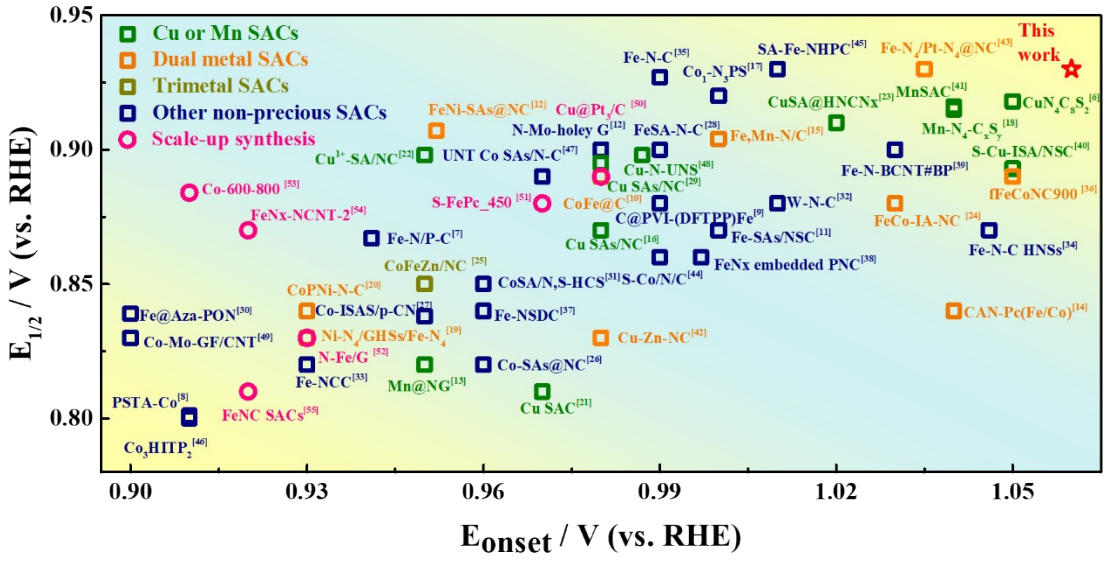

Figure S25. Comparison of E_{onset} and $E_{1/2}$ values between our catalyst and some recent reported ORR catalysts in alkaline media. [1–50]

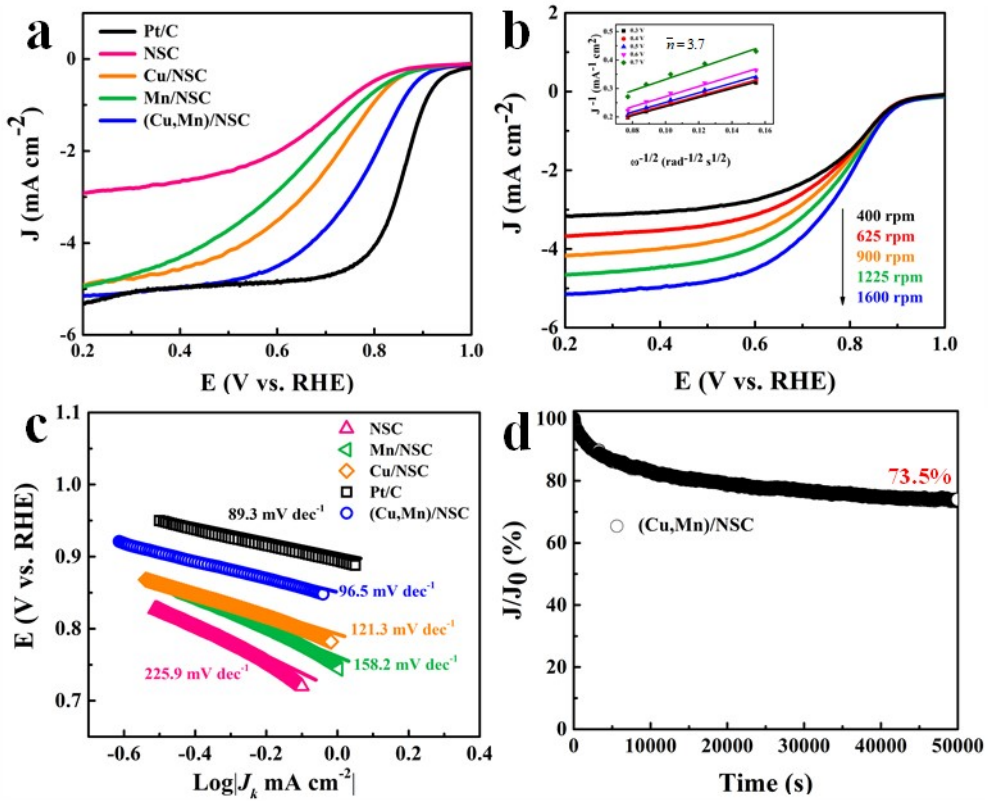

Figure S26. Electrocatalytic ORR performance of (Cu,Mn)/NSC in 0.1 M $HClO_4$ solution. (a) ORR polarization curves for NSC, Cu/NSC, Mn/NSC, (Cu,Mn)/NSC and Pt/C. (b) ORR polarization curves of (Cu,Mn)/NSC at different rotating rates (inset: K-L plots and electron transfer numbers). (c) Tafel slopes of different catalysts. (d) Current−time chronoamperometric responses of (Cu,Mn)/NSC.

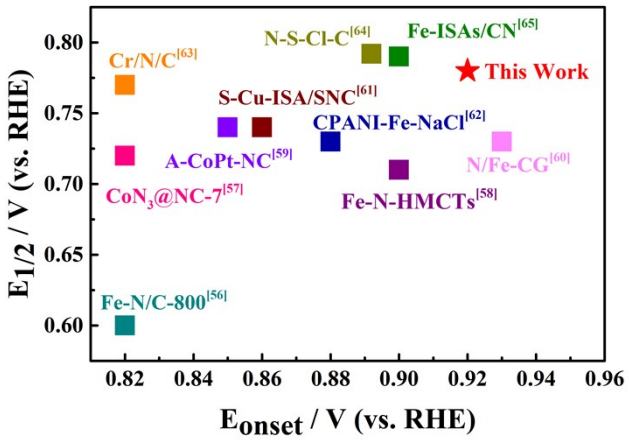

Figure S27. Comparison of E_{onset} and $E_{1/2}$ values between our catalyst and some recent reported ORR catalysts in acid media.[51–60]

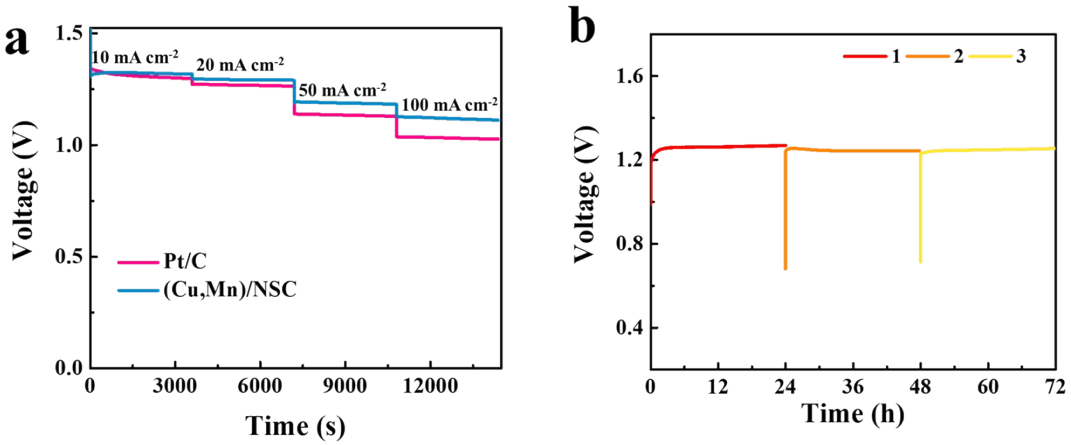

Figure S28. (a) galvanostatic discharge curves at various current densities (10, 20, 50 and 100 mA cm^{-2}) (b) Long-time durability of the primary Zn-air battery using (Cu,Mn)/NSC at 10 mA cm^{-2}. The battery can be mechanically recharged by refilling KOH electrolyte and replacing the Zn plate to regenerate the Zn–air battery.

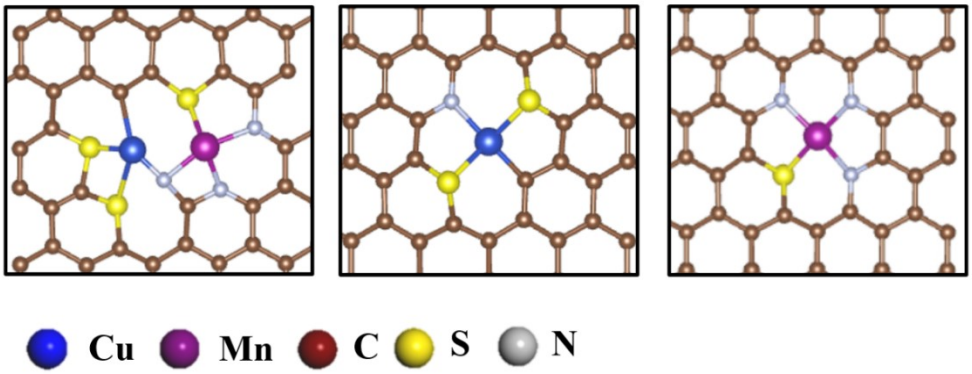

Figure S29. Optimized structure models for (Cu,Mn)/NSC (Cu,Mn-$N_3S_3C_1$), Cu/NSC (Cu-$N_1S_2C_1$), and Mn/NSC (Mn-N_3S_1)

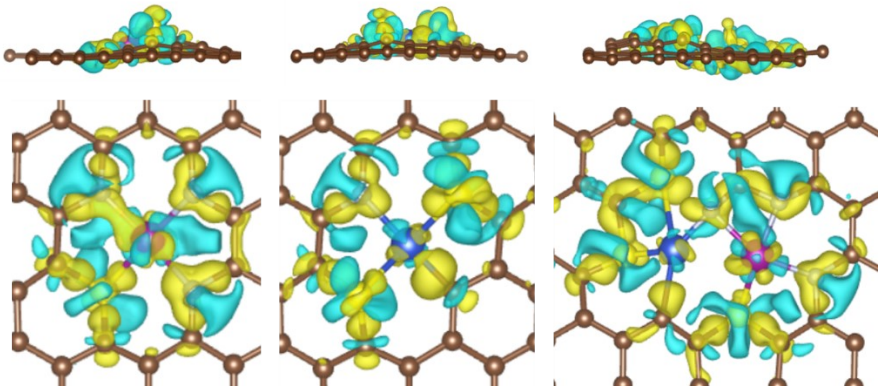

Figure S30 Calculated charge transfer differences of Mn-N_3S_1, Cu-$N_1S_2C_1$ and Cu,Mn-$N_3S_3C_1$ site (from left to right), where the iso-surface value is set to be 0.008 e/$Å^3$ and the yellow and cyan parts indicate the charge accumulation and depletion, respectively.

Table S5. Calculated Bader charge (unit: e) for metal atoms in (Cu,Mn)/NSC (Cu,Mn-$N_3S_3C_1$), Cu/NSC (Cu-$N_1S_2C_1$) and Mn/NSC (Mn-N_3S_1).

Structures	Mn	Cu
Mn/NSC	7.115	/
Cu/NSC	/	10.986
(Cu,Mn)/NSC	7.063[1]	10.960[1]

[1] In the pseudopotential during DFT calculation, the number of extranuclear electrons of Mn and Cu is 7 and 11 electrons, respectively. Obviously, in (Cu,Mn)/NSC system, the calculated Bader charge of Cu atoms is 10.960 (＜11) while the calculated Bader charge of Mn atoms is 7.063 (＞7), suggesting that the Cu atoms transferred electrons to Mn atoms and playing the role as the electron donors.

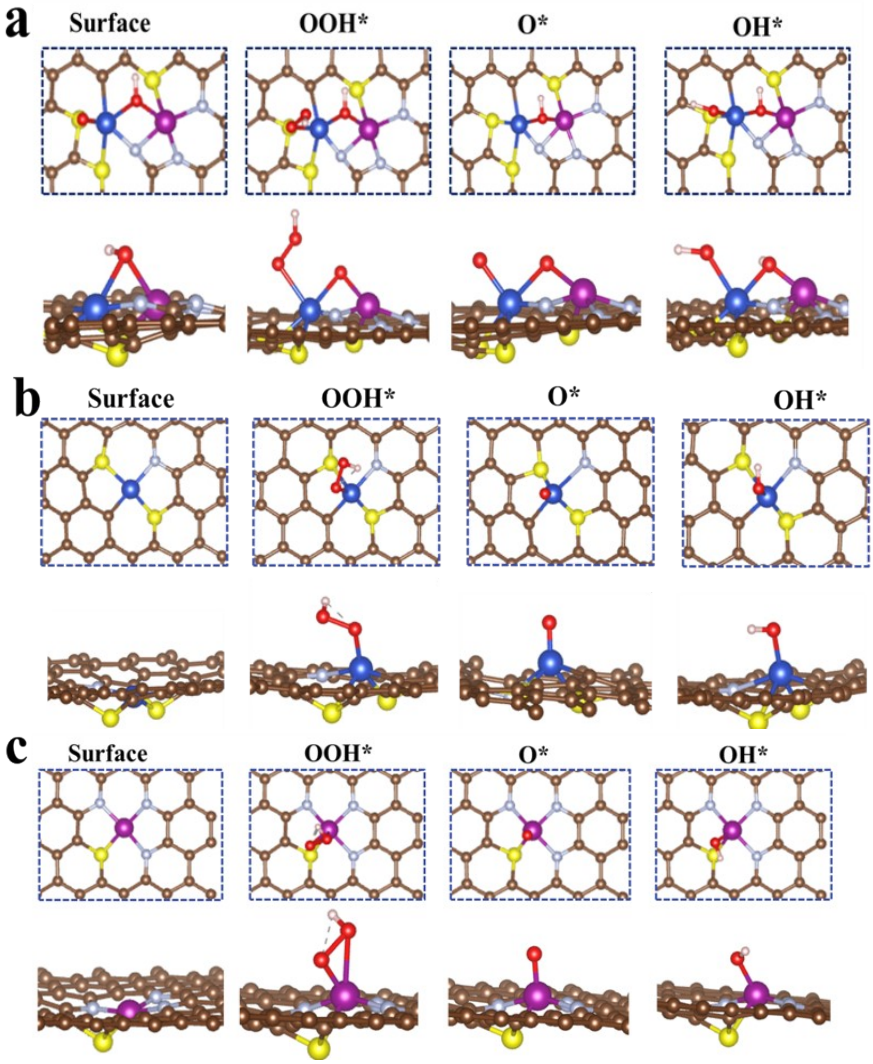

Figure S31. Structure models of oxygen intermediates adsorbed on (a) Cu site on (Cu,Mn)/NSC (Cu,Mn-$N_3S_3C_1$), (b) Cu/NSC (Cu-$N_1S_2C_1$) and (c) Mn/NSC (Mn-N_3S_1). Brown, gray, yellow, blue, purple, and red balls are C, N, S, Cu, Mn, and O atoms, respectively.

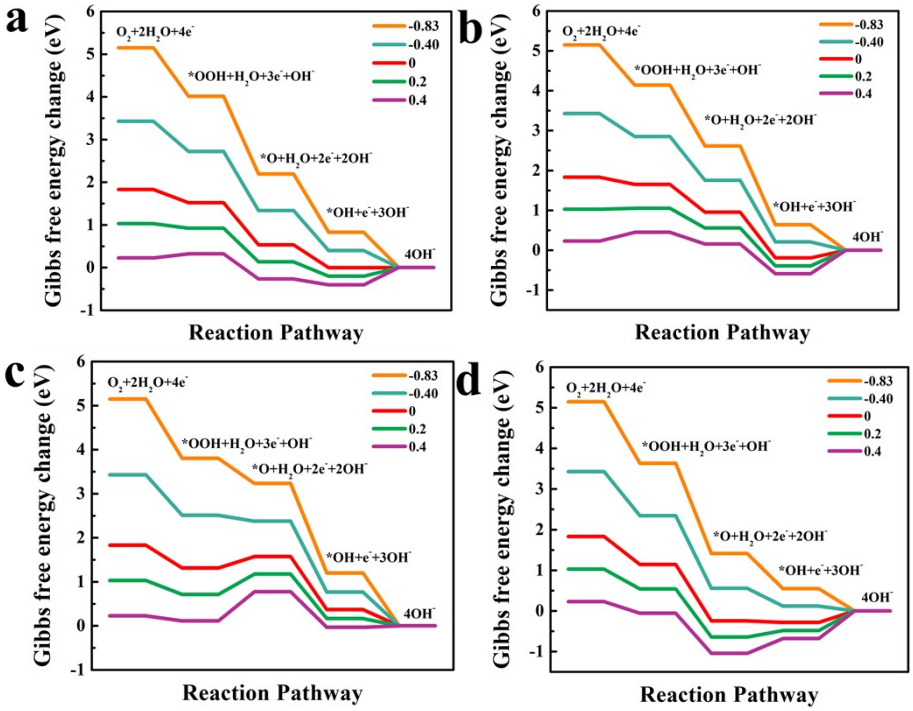

Figure S32. Free energy diagram for ORR on (a) Mn site in (Cu,Mn)/NSC (Cu,Mn-$N_3S_3C_1$), (b) Cu site in (Cu,Mn)/NSC (Cu,Mn-$N_3S_3C_1$), (c) Cu/NSC (Cu-$N_1S_2C_1$) and (d) Mn/NSC (Mn-N_3S_1) at different potentials in alkaline media.

REFERENCES

1 Z. Jiang, W. Sun, H. Shang, W. Chen, T. Sun, H. Li, J. Dong, J. Zhou, Z. Li, Y. Wang, R. Cao, R. Sarangi, Z. Yang, D. Wang, J. Zhang and Y. Li, *Energy Environ. Sci.*, 2019, **12**, 3508–3514.

2 K. Yuan, D. Lützenkirchen-Hecht, L. Li, L. Shuai, Y. Li, R. Cao, M. Qiu, X. Zhuang, M. K. H. Leung, Y. Chen and U. Scherf, *J. Am. Chem. Soc.*, 2020, **142**, 2404–2412.

3 X. Wei, D. Zheng, M. Zhao, H. Chen, X. Fan, B. Gao, L. Gu, Y. Guo, J. Qin, J. Wei, Y. Zhao and G. Zhang, *Angew. Chemie Int. Ed.*, 2020, **59**, 14639–14646.

4 Y. M. Zhao, P. C. Zhang, C. Xu, X. Y. Zhou, L. M. Liao, P. J. Wei, E. Liu, H. Chen, Q. He and J. G. Liu, *ACS Appl. Mater. Interfaces*, 2020, **12**, 17334–17342.

5 C. Xu, L. Chen, Y. Wen, S. Qin, H. Li, Z. Hou, Z. Huang, H. Zhou and Y. Kuang, *Mater. Today Energy*, 2021, **21**, 100721.

6 J. Zhang, Y. Zhao, C. Chen, Y. C. Huang, C. L. Dong, C. J. Chen, R. S. Liu, C. Wang, K. Yan, Y. Li and G. Wang, *J. Am. Chem. Soc.*, 2019, **141**, 20118–20126.

7 F. Luo, J. Zhu, S. Ma, M. Li, R. Xu, Q. Zhang, Z. Yang, K. Qu, W. Cai and Z. Chen, *Energy Storage Mater.*, 2021, **35**, 723–730.

8 P. Du, K. Hu, J. Lyu, H. Li, X. Lin, G. Xie, X. Liu, Y. Ito and H. J. Qiu, *Appl. Catal. B Environ.*, 2020, **276**, 119172.

9 S. Yang, Y. Yu, M. Dou, Z. Zhang, L. Dai and F. Wang, *Angew. Chemie - Int. Ed.*, 2019, **58**, 14724–14730.

10 S. Gong, C. Wang, P. Jiang, L. Hu, H. Lei and Q. Chen, *J. Mater. Chem. A*, 2018, **6**, 13254–13262.
11 S. Ma, Z. Han, K. Leng, X. Liu, Y. Wang, Y. Qu and J. Bai, *Small*, 2020, **16**, 2001384.
12 Y. Chen, R. Gao, S. Ji, H. Li, K. Tang, P. Jiang, H. Hu, Z. Zhang, H. Hao, Q. Qu, X. Liang, W. Chen, J. Dong, D. Wang and Y. Li, *Angew. Chemie - Int. Ed.*, 2021, **60**, 3212–3221.
13 H. Shang, Z. Jiang, D. Zhou, J. Pei, Y. Wang, J. Dong, X. Zheng, J. Zhang and W. Chen, *Chem. Sci.*, 2020, **11**, 5994–5999.
14 J. Chen, H. Li, C. Fan, Q. Meng, Y. Tang, X. Qiu, G. Fu and T. Ma, 2020, **2003134**, 1–11.
15 Z. Li, H. He, H. Cao, S. Sun, W. Diao, D. Gao, P. Lu, S. Zhang, Z. Guo, M. Li, R. Liu, D. Ren, C. Liu, Y. Zhang, Z. Yang, J. Jiang and G. Zhang, *Appl. Catal. B Environ.*, 2019, **240**, 112–121.
16 L. Cui, L. Cui, Z. Li, J. Zhang, H. Wang, S. Lu and Y. Xiang, *J. Mater. Chem. A*, 2019, **7**, 16690–16695.
17 T. Sun, Y. Li, T. Cui, L. Xu, Y. G. Wang, W. Chen, P. Zhang, T. Zheng, X. Fu, S. Zhang, Z. Zhang, D. Wang and Y. Li, *Nano Lett.*, 2020, **20**, 6206–6214.
18 N. K. Wagh, S. S. Shinde, C. H. Lee, J. Y. Jung, D. H. Kim, S. H. Kim, C. Lin, S. U. Lee and J. H. Lee, *Appl. Catal. B Environ.*, 2020, **268**, 118746.
19 L. Chen, Y. Zhang, L. Dong, W. Yang, X. Liu, L. Long, C. Liu, S. Dong and J. Jia, *J. Mater. Chem. A*, 2020, **8**, 4369–4375.
20 J. Wang, W. Zang, S. Xi, M. Kosari, S. J. Pennycook and H. C. Zeng, *J. Mater. Chem. A*, 2020, **8**, 17266–17275.
21 X. Han, X. Ling, Y. Wang, T. Ma, C. Zhong, W. Hu and Y. Deng, *Angew. Chemie - Int. Ed.*, 2019, **58**, 5359–5364.
22 A. Han, W. Chen, S. Zhang, M. Zhang, Y. Han, J. Zhang, S. Ji, L. Zheng, Y. Wang, L. Gu, C. Chen, Q. Peng, D. Wang and Y. Li, *Adv. Mater.*, 2018, **30**, 1–7.
23 L. Jiao, R. Zhang, G. Wan, W. Yang, X. Wan, H. Zhou, J. Shui, S.-H. Yu and H.-L. Jiang, *Nat. Commun.*, 2020, **11**, 2831.
24 H. Wang and S. Lu, , DOI:10.1039/C9TA03518D.
25 S. J. Kim, J. Mahmood, C. Kim, G. F. Han, S. W. Kim, S. M. Jung, G. Zhu, J. J. De Yoreo, G. Kim and J. B. Baek, *J. Am. Chem. Soc.*, 2018, **140**, 1737–1742.
26 Z. Zhang, X. Zhao, S. Xi, L. Zhang, Z. Chen, Z. Zeng, M. Huang, H. Yang, B. Liu, S. J. Pennycook and P. Chen, *Adv. Energy Mater.*, 2020, **10**, 2002896.
27 Z. Chen, W. Gong, Z. Liu, S. Cong, Z. Zheng, Z. Wang, W. Zhang, J. Ma, H. Yu, G. Li, W. Lu, W. Ren and Z. Zhao, *Nano Energy*, 2019, **60**, 394–403.
28 N. Jia, Q. Xu, F. Zhao, H. X. Gao, J. Song, P. Chen, Z. An, X. Chen and Y. Chen, *ACS Appl. Energy Mater.*, 2018, **1**, 4982–4990.
29 Y. Chen, Z. Li, Y. Zhu, D. Sun, X. Liu, L. Xu and Y. Tang, *Adv. Mater.*, 2019, **31**, 1–8.
30 C. Zhu, Q. Shi, B. Z. Xu, S. Fu, G. Wan, C. Yang, S. Yao, J. Song, H. Zhou, D. Du, S. P. Beckman, D. Su and Y. Lin, *Adv. Energy Mater.*, 2018, **8**, 1801956.
31 G. Zhang, Y. Jia, C. Zhang, X. Xiong, K. Sun, R. Chen, W. Chen, Y. Kuang, L. Zheng, H. Tang, W. Liu, J. Liu, X. Sun, W. F. Lin and H. Dai, *Energy Environ. Sci.*, 2019, **12**, 1317–1325.
32 J. Zhang, M. Zhang, Y. Zeng, J. Chen, L. Qiu, H. Zhou, C. Sun, Y. Yu, C. Zhu and Z. Zhu, *Small*, 2019, **15**, 1900307.

33 L. Ma, S. Chen, Z. Pei, Y. Huang, G. Liang, F. Mo, Q. Yang, J. Su, Y. Gao, J. A. Zapien and C. Zhi, *ACS Nano*, 2018, **12**, 1949–1958.

34 E. Li, F. Yang, Z. Wu, Y. Wang, M. Ruan, P. Song, W. Xing and W. Xu, *Small*, 2018, **14**, 1702827.

35 H. Shang, X. Zhou, J. Dong, A. Li, X. Zhao, Q. Liu, Y. Lin, J. Pei, Z. Li, Z. Jiang, D. Zhou, L. Zheng, Y. Wang, J. Zhou, Z. Yang, R. Cao, R. Sarangi, T. Sun, X. Yang, X. Zheng, W. Yan, Z. Zhuang, J. Li, W. Chen, D. Wang, J. Zhang and Y. Li, *Nat. Commun.*, 2020, **11**, 3049.

36 H. Shang, W. Sun, R. Sui, J. Pei, L. Zheng, J. Dong, Z. Jiang, D. Zhou, Z. Zhuang, W. Chen, J. Zhang, D. Wang and Y. Li, *Nano Lett.*, 2020, **20**, 5443–5450.

37 M. Tong, F. Sun, Y. Xie, Y. Wang, Y. Yang, C. Tian, L. Wang and H. Fu, *Angew. Chemie Int. Ed.*, 2021, **60**, 14005–14012.

38 A. Han, X. Wang, K. Tang, Z. Zhang, C. Ye, K. Kong, H. Hu, L. Zheng, P. Jiang, C. Zhao, Q. Zhang, D. Wang and Y. Li, *Angew. Chemie*, 2021, **133**, 19411–19420.

39 T. Sun, W. Zang, H. Yan, J. Li, Z. Zhang, Y. Bu, W. Chen, J. Wang, J. Lu and C. Su, *ACS Catal.*, 2021, **11**, 4498–4509.

40 G. Chen, P. Liu, Z. Liao, F. Sun, Y. He, H. Zhong, T. Zhang, E. Zschech, M. Chen, G. Wu, J. Zhang and X. Feng, *Adv. Mater.*, , DOI:10.1002/adma.201907399.

41 Y. Lian, W. Yang, C. Zhang, H. Sun, Z. Deng, W. Xu, L. Song, Z. Ouyang, Z. Wang, J. Guo and Y. Peng, *Angew. Chemie Int. Ed.*, 2020, **59**, 286–294.

42 X. Sun, S. Sun, S. Gu, Z. Liang, J. Zhang, Y. Yang, Z. Deng, P. Wei, J. Peng, Y. Xu, C. Fang, Q. Li, J. Han, Z. Jiang and Y. Huang, *Nano Energy*, 2019, **61**, 245–250.

43 Y. Guan, N. Li, Y. Li, L. Sun, Y. Gao, Q. Zhang, C. He, J. Liu and X. Ren, *Nanoscale*, 2020, **12**, 14259–14266.

44 M. Tavakkoli, E. Flahaut, P. Peljo, J. Sainio, F. Davodi, E. V. Lobiak, K. Mustonen and E. I. Kauppinen, *ACS Catal.*, 2020, **10**, 4647–4658.

45 M. Luo, L. Wei, F. Wang, K. Han and H. Zhu, *J. Power Sources*, 2014, **270**, 34–41.

46 S. Ratso, A. Zitolo, M. Käärik, M. Merisalu, A. Kikas, V. Kisand, M. Rähn, P. Paiste, J. Leis, V. Sammelselg, S. Holdcroft, F. Jaouen and K. Tammeveski, *Renew. Energy*, 2021, **167**, 800–810.

47 J. Wang, H. Zhang, C. Wang, Y. Zhang, J. Wang, H. Zhao, M. Cheng, A. Li and J. Wang, *Energy Storage Mater.*, 2018, **12**, 1–7.

48 T. Cao, D. Wang, J. Zhang, C. Cao and Y. Li, *Chem. - A Eur. J.*, 2015, **21**, 14022–14029.

49 Y. Li, H. Huang, S. Chen, C. Wang and T. Ma, *Chem. - A Eur. J.*, 2019, **25**, 2637–2644.

50 J. Ma, L. Wang, Y. Deng, W. Zhang, T. Wu and Y. Song, *Sci. China Mater.*, 2021, **64**, 631–641.

51 L. Lin, Q. Zhu and A. W. Xu, *J. Am. Chem. Soc.*, 2014, **136**, 11027–11033.

52 S. Lai, L. Xu, H. Liu, S. Chen, R. Cai, L. Zhang, W. Theis, J. Sun, D. Yang and X. Zhao, *J. Mater. Chem. A*, 2019, **7**, 21884–21891.

53 X. Cui, L. Gao, S. Lei, S. Liang, J. Zhang, C. D. Sewell, W. Xue, Q. Liu, Z. Lin and Y. Yang, *Adv. Funct. Mater.*, 2021, **31**, 2009197.

54 L. Zhang, J. M. T. A. Fischer, Y. Jia, X. Yan, W. Xu, X. Wang, J. Chen, D. Yang, H. Liu, L. Zhuang, M. Hankel, D. J. Searles, K. Huang, S. Feng, C. L. Brown and X. Yao, *J. Am. Chem. Soc.*, 2018, **140**, 10757–10763.

55 B. Li, S. P. Sasikala, D. H. Kim, J. Bak, I. D. Kim, E. A. Cho and S. O. Kim, *Nano Energy*, 2019, **56**, 524–530.

56 H. Shang, X. Zhou, J. Dong, A. Li, X. Zhao, Q. Liu, Y. Lin, J. Pei, Z. Li, Z. Jiang, D. Zhou, L. Zheng, Y. Wang, J. Zhou, Z. Yang, R. Cao, R. Sarangi, T. Sun, X. Yang, X. Zheng, W. Yan, Z. Zhuang, J. Li, W. Chen, D. Wang, J. Zhang and Y. Li, *Nat. Commun.*, 2020, **11**, 1–11.
57 W. Ding, L. Li, K. Xiong, Y. Wang, W. Li, Y. Nie, S. Chen, X. Qi and Z. Wei, *J. Am. Chem. Soc.*, 2015, **137**, 5414–5420.
58 E. Luo, H. Zhang, X. Wang, L. Gao, L. Gong, T. Zhao, Z. Jin, J. Ge, Z. Jiang, C. Liu and W. Xing, *Angew. Chemie*, 2019, **131**, 12599–12605.
59 Y. Shen, Y. Li, G. Yang, Q. Zhang, H. Liang and F. Peng, *J. Energy Chem.*, 2020, **44**, 106–114.
60 Y. Chen, S. Ji, Y. Wang, J. Dong, W. Chen, Z. Li, R. Shen, L. Zheng, Z. Zhuang, D. Wang and Y. Li, *Angew. Chemie - Int. Ed.*, 2017, **56**, 6937–6941.